CHEMISTRY OF MATERIALS

Article

pubs.acs.org/cm

# Vapor Phase Synthesis of Conducting Polymer Nanocomposites Incorporating 2D Nanoparticles

Nastasja Vucaj,[†] Matthew D. J. Quinn,[‡] Curdin Baechler,[§] Shannon M. Notley,[‡] Philip Cottis,[∥] Pejman Hojati-Talemi,[⊥] Manrico V. Fabretto,[⊥] Gordon G. Wallace,[#] Peter J. Murphy,[⊥] and Drew R. Evans*,[⊥]

[†]Fakultät Angewandte Chemie, University of Reutlingen, Reutlingen, 72762 Germany

[‡]Department of Chemistry and Biotechnology, Faculty of Science, Engineering and Technology, Swinburne University of Technology, Hawthorn, Victoria 3122, Australia

[§]Laboratory of Mechanical Systems Engineering, EMPA, Überlandstrasse 129, Dübendorf, 8600 Switzerland

[∥]Department of Chemistry, University of Bath, Bath BA2 7AY, United Kingdom

[⊥]Thin Film Coatings Group, Mawson Institute, University of South Australia, Mawson Lakes, South Australia 5095, Australia

[#]ARC Centre of Excellence for Electromaterials Science, Intelligent Polymer Research Institute, University of Wollongong, Wollongong, New South Wales 2522, Australia

Supporting Information

**ABSTRACT:** The one step fabrication of nanocomposite films of conducting polymers with 2D nanoparticles is investigated in this study. Specifically, the inclusion of nanomaterials (single layer graphene, single layer molybdenum disulfide) within PEDOT is achieved using the vapor phase polymerization (VPP) technique. This facile process allows for the formation of thin films of the order of less than 200 nm, which display a wide range of enhanced properties (mechanical, optical, and electrochemical). Herein, in a typical example with added graphene (<0.003% w/w), the in-plane modulus of the film is increased to 145 GPa (ca. 65% increase above PEDOT−Tos) without any decrease in light transmission or lowering of conductivity. Furthermore, the nanocomposite outperforms both the PEDOT−Tos film and a Pt substrate in the reduction of oxygen when acting as an air-electrode.

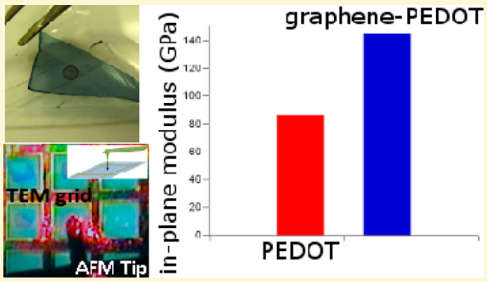


## INTRODUCTION

Composite materials have become widely used in industrial applications due to their relative ease of manufacture, engineered properties, and performance.[1,2] An exciting extension of the composite materials application is the generation of thin films which has allowed novel applications to be developed such as devices and sensors. A nanocomposite thin film comprises nanoparticles or nanomaterials (such as 2D materials) dispersed throughout a continuous matrix. The overall film thickness of the thin film composites is generally less than 1−2 $\mu$m, typically on the order of only a few hundred nanometers. To generate the specific properties of the film, reliance is placed on the complex interaction between the dispersed materials and the continuous matrix to external stimuli such as light, electric fields, or mechanical loads. Some of the properties that such films may possess are high hardness,[3] low gas permeability,[4] high conductivity,[5] high dielectric constant,[6] electroluminescence,[7] and/or photoconductivity.[8] These properties, in isolation or in combinations thereof, allow the nanocomposite thin films to impart protective or functional behavior to the device in which they are incorporated.

Layered materials represent a diverse and largely untapped source of two-dimensional (2D) systems, which can be efficiently dispersed in common solvents and can be formed into films,[9−12] for fabrication into complex structures.[13] The best known 2D nanomaterial in this sense is graphene, a monolayer of $sp^2$-hybridized carbon atoms arranged in a 2D lattice, known for its exceptional mechanical and electrical properties.[14] Several studies have demonstrated that graphene embedded within a polymer matrix can drastically change and enhance the thin film performance.[15−17] In the wake of graphene, many other 2D nanomaterials are gaining increasing interest in the research community, such as the dichalcogenides and, in particular, molybdenum disulfide ($MoS_2$).[18−20] Bulk $MoS_2$ is a "'layered'" transition metal dichalcogenide semiconductor with an indirect band gap[21] and has attracted interest as a material for enhancing photovoltaic and photocatalytic devices.[22,23] Mo and S atoms form a trilayer stack to give S−Mo−S sandwiches coordinated in a triangular prismatic fashion,

Received: April 23, 2014
Revised: June 24, 2014
Published: June 24, 2014

   dx.doi.org/10.1021/cm5014653 | Chem. Mater. 2014, 26, 4207−4213

held together by weak interlayer bonds.[24,25] Single layers of $MoS_2$ have a large intrinsic bandgap of 1.98 eV, though the reported mobilities are too low for practical devices.[13,18−20,26]

With respect to nanocomposite thin films, not only does the filler material play an important role but also the matrix or host material. The conducting polymer poly(3,4-ethylenedioxythiophene), PEDOT, is one example of such a host material, displaying high conductivity,[27] high electrocatalytic efficiency,[28,29] and electrochromic behavior.[30,31] The majority of studies focus on PEDOT nanocomposites fabricated via solution based processes.[32−34] For example, Hong et al. fabricated counter electrodes for dye-sensitized solar cells using thin films fabricated with 1 wt % transparent graphene and commercially available PEDOT doped with poly(styrenesulfonate) (PSS).[32] In contrast, Choi et al. employed a layer-by-layer assembly technique with PEDOT:PSS and graphene to create multilayer thin films with enhanced conductivity for ubiquitous use in organic electronic devices.[33] The overall conductivity for this multilayer structure of graphene−PEDOT:PSS−graphene was reported as 12 S/cm. In addition to PEDOT, poly(pyrrole) (PPy) has been considered as a promising host material, for example, in supercapacitors owing to its excellent energy storage capacity.[35,36] The work of Konwer et al. led to PPy-based nanocomposites with elevated electrical conductivity approaching 80 S/cm, in contrast to the 7 S/cm obtained by Zhang et al. Similarly, PPy−graphene nanocomposites fabricated by in situ synthesis of graphene oxide in the presence of a pyrrole monomer, followed by chemical reduction, produced a material with comparable conductivity (2 to 8 S/cm)[37] to that of the aforementioned graphene−PEDOT:PSS.

Despite advances in the synthesis of nanocomposite thin films of conducting polymers containing 2D nanomaterials, the overall conductivity is well short of those achieved for thin film PEDOT synthesized using vapor phase polymerization (VPP).[38] Fabretto et al.[31,39,40] utilize poly(ethylene glycol−propylene glycol−ethylene glycol) (PEG−PPG−PEG) copolymers in the VPP process to create uniform large area PEDOT films with conductivity up to 3400 S/cm.[27] Such VPP PEDOT is typically doped with tosylate (Tos) anions, which when combined with well-ordered polymer chains yields a material recently shown to be a semimetal.[41] Very recently, attempts have been made to incorporate graphene into PEDOT−Tos via the VPP process by Yang et al.[42] Such composite films, when deposited on glass substrates, returned electrical conductivity values of 220 ± 20 S/cm. In Tung et al.'s work, a thin hybrid film of reduced graphene oxide and PEDOT−Tos was fabricated by means of VPP as the active material in chemical sensors.[43] These thin hybrid films are estimated to have an electrical conductivity on the order of 1 S/cm, derived from the geometry of the interdigit electrode architecture employed, a hybrid film thickness of 30 nm, and a resistance of ca. 100 kΩ. Attempts to create nanocomposites via VPP have yet to realize conductivities of greater than 1000 S/cm, thus failing to deliver advanced materials for ubiquitous employment across a multitude of different organic electronic devices.

In this study, $MoS_2$ and graphene 2D nanoparticles (exfoliated in a water solution containing a triblock copolymer)[26,44] were dispersed in an oxidant solution used to synthesize highly conductive composites with PEDOT−Tos via VPP. These nanocomposite thin films were then assessed in relation to their electrical properties and shown to be superior to previously reported nanocomposites. Furthermore, owing to their stability, the graphene variants were investigated with respect to their mechanical properties and electrocatalytic performance.

## MATERIALS AND METHODS

**Preparation of 2D Nanomaterial Dispersions.** The 2D materials incorporated within the thin films were produced via liquid phase exfoliation with continuous surfactant addition.[18,26,44] This method is capable of producing substantial concentrations of monolayer sheets from bulk starting materials such as the production of monolayer graphene sheets from bulk powdered graphite.

Separation of the sheets can be readily achieved through sonication by approximately matching the interfacial tension of the liquid phase to the surface energy between the sheets. The addition of an optimized concentration of surfactant, such as the triblock copolymer P123 ($PEG_{20}$:$PPG_{70}$:$PEG_{20}$ $M_W$ ∼5750 Da.) is employed to decrease the surface tension of the aqueous phase to approximately 41 mJ/m$^2$ and achieve the matching of the cohesive energies.

The surfactant plays a dual role during exfoliation by both lowering the interfacial tension as well as sterically stabilizing the sheets to aid in their dispersion within the suspension. The free surfactant in solution adsorbs to the rapidly increasing available surface area, depleting it from solution. The exposed hydrophilic segments (PEG) of the surfactant adsorbed to the sheets act to prevent aggregation through repulsive steric interactions.

The surfactant is removed from the suspension as it is adsorbed to the exfoliated sheets, which results in an increase in surface tension. This shift of the surface tension and loss of the approximate matching of the cohesive energies subsequently halts any further exfoliation. The optimum surfactant concentration can be maintained by continuously adding the surfactant into the sonication vessel, and far greater concentrations of the monolayer sheets can be achieved.

Powdered molybdenum(IV) sulfide ($MoS_2$; Sigma-Aldrich, Sydney) and powdered graphite (Ajax Chemicals, Sydney) both with a bulk particle size of less than 2 μm were used as received, and all suspensions were prepared in Milli-Q filtered water. The surfactant employed for both materials was the triblock copolymer P123 (Sigma-Aldrich, Sydney) and was used as received. The bulk layered material (1% w/w), surfactant, and Milli-Q are combined in a 10 L reaction reservoir, and a drip feed of diluted surfactant is added over the course of the sonication period. A pump system was established to cycle the suspension to the Q700 Qsonica ultrasonicator (probe model CL-334) and back to the reaction reservoir.

Following exfoliation, the suspensions were centrifuged at 1500 rpm for 5 min using the Rotofix 32 (Hettich) to remove the larger, unexfoliated particles. The supernatant is then extracted; the sample concentration of single and few-layered sheets was determined via UV−visible spectrophotometry (Figure S1). Graphene was determined to be 0.015% w/w in the suspension and $MoS_2$ to be 0.0065% w/w (using literature values for the extinction coefficients[26,45−47]).

In order to confirm the successful exfoliation, the samples are characterized via Raman spectroscopy, which can definitively indicate the presence of monolayer or few layer sheets as well as any sheet defects (Figure S2). Graphene can be readily identified by the peak at 2675 cm$^{-1}$, as the position and shape of this peak can indicate the number of graphene layers.[44] Sheet thickness of the $MoS_2$ can be confirmed by the positioning of the $A_{1g}$ and $E_{2g}{}^1$ peaks located at approximately 405 and 380 cm$^{-1}$, respectively (532 nm excitation).[26]

**Preparation of Oxidant Solutions Containing Nanomaterial.** Fe(III) tosylate ($Fe(Tos)_3$) was received from HC Stark as a 40 wt % CB40 solution in n-butanol. A series of oxidant solutions was prepared using the pristine oxidant solution and diluting to 16 wt % $Fe(Tos)_3$ using a solution of 2D nanomaterial diluted in ethanol and Milli-Q water. This diluent solution contained the following weight ratios of 2D nanomaterial dispersion to ethanol to Milli-Q water: 70/30/0, 56/30/14, 35/30/35, 14/30/56, and 0/30/70. This resulted in oxidant solutions containing nominal 2D nanomaterial loadings of graphene, 0.00255% w/w, 0.00210% w/w, 0.00135% w/w, and 0.00045% w/w


dx.doi.org/10.1021/cm5014653 | Chem. Mater. 2014, 26, 4207−4213

and $MoS_2$, 0.00111% w/w, 0.00091% w/w, 0.00059% w/w, and 0.00020% w/w, with 0% used as a reference samples in both cases.

The sterically stabilized graphene and $MoS_2$ dispersed well in the oxidant solution, with little to no agglomeration observed (Figure S6). The oxidant solution showed a gradual change in visual appearance (color) as the loading of nanomaterial was increased. With an increasing amount of nanoparticle dispersion, the color of the solution changed from a dark orange-brownish (typical of neat oxidant) to dark green. The solutions of graphene show a darker color and are more viscous compared to the solutions of $MoS_2$. This color change was confirmed not to arise from the oxidation of the 2D nanomaterials in the presence of $Fe(Tos)_3$ (Figure S6), through observation of absorbance peaks assigned to Fe(III) (Fe(II) shows minimal absorbance in the same spectral range[48]). In the experiment, the nanomaterials were exposed to the oxidant for much longer timeframes than experienced in the VPP process without a loss of the Fe(III) absorbance. Irrespective of the concentration of graphene, the 2D nanomaterials remained well dispersed in the oxidant solution for up to 3 h without any visible agglomeration; even after 1 day, the graphene weakly flocculated and could be easily redispersed upon agitation.

**Synthesis of Nanocomposite Thin Films.** 3,4-Ethylenedioxythiophene (EDOT) monomer was obtained from Aldrich. After the addition of the 2D nanomaterial dispersions into the oxidant solution, oxidant thin films were deposited on glass microscope slides and then exposed to the VPP process. The glass substrates (prior to coating) were washed using a mild detergent and then ethanol and finally rinsed using high purity water. Prior to spin-coating, the substrates were air plasma treated (Diener, Plasma etcher NANO, Germany) for 2 min. The oxidant solution was spin-coated (400B-6NPP, Laurell Technologies Inc.) at a speed of 1500 rpm for 25 s and then placed on a 70 °C hot plate for 30 s. Immediately after heating, samples were placed into a 115 L vacuum chamber oven (Binder, Germany) set to 35 °C. The chamber was pumped down to 45 mbar, at which time the vessel containing the EDOT monomer (heated to 45 °C) was opened, releasing monomer vapor into the volume of the chamber. Samples were removed after 25 min (typical polymerization time) and placed on a 70 °C hot plate for 2 min to anneal the polymer. Furthermore, this annealing prevents stress fracturing during the ethanol-washing step. Samples were removed from the hot plate and further annealed through cooling to room temperature. After 20 min, samples under general lab conditions (25 °C and 35% RH) were carefully rinsed in an ethanol bath to remove consumed and unconsumed oxidant, unbound surfactant, and residual unreacted monomer. At the end, samples were dried with an air gun, followed by a final ethanol spray rinse and air-drying step.

To test the oxygen reduction reaction (ORR) efficiency of these nanocomposite films, graphene−PEDOT−Tos (0.00255% w/w graphene in the oxidant solution) and PEDOT−Tos only films were deposited onto 0.45 $\mu$m PVDF membranes used to prepare the air electrodes, as described elsewhere.[29] A PVDF membrane was saturated with paraffin wax dissolved in minimal *n*-hexane and then dried at room temperature. After VPP, the membranes were soaked in hexane for 15 min to remove the wax, dried, and then soaked in ethanol for 30 min to remove any oxidant and remaining monomer before being dried again. Both drying steps occurred on 70 °C hot plates for a 30 min period. To achieve multilayer electrodes, membranes were rinsed only with ethanol and then dried before repeating oxidant coating and VPP steps. Pt was sputtered onto the same PVDF membrane for comparison purposes.

**Analysis of Nanocomposite Thin Films.** The resulting conducting polymer thin films with and without 2D nanomaterials were characterized by a variety of different techniques. Morphology and structure were observed using both AFM (Integra, NT-MDT) and SEM (FEI Quanta 400 microscope, 20 kV), with compressive mechanical testing performed using the same AFM. The AFM cantilever spring constant was measured using the Sader method.[49] Copper transmission electron microscope (TEM) grids, 200-mesh grid, were purchased from SPI supplies, for creating the drum-like structure comprised of the thin film samples stretched across the upper surface of the TEM grid. In-plane modulus measurements were determined by conducting AFM force curve measurements on the conducting polymer thin film at the center of each TEM grid (where AFM imaging prior to force curves was used to determine the center).

Techniques to characterize the graphene−PEDOT−Tos thin films, to indirectly determine the presence of graphene include thermogravimetric analysis (TGA-2950, TA Instruments), XRD (Bruker D8 Advance with Cu K □), and Raman (300A Raman system from WITEC with laser excitation at 532 nm).

Electrical analysis of the thin films was conducted using the four-point probe technique (multi-height probe, RM3, Jandel Engineering). The sheet resistance ($R_s$) of the samples in Ω/square was measured with a tip radius of 100 $\mu$m, tip spacing of 1 mm, and 60 g preset load. On each sample, 10 measurements were taken and the average value reported. The conductivity ($\sigma$) in S/cm was calculated with the following equation:

$$\sigma = (R_s.\ t)^{-1} \tag{1}$$

where $t$ is the thickness of the sample in centimeters.

The influence of pH on the stability of the nanocomposite thin films was studied by soaking the respective films in either 20% KOH (in Milli-Q water) or 1 M $H_2SO_4$. Both KOH pellets and $H_2SO_4$ liquid were purchased and used as is from Sigma-Aldrich.

The ORR efficiency was observed for the samples deposited on the PVDF membranes using the cell architecture described elsewhere[29] and measuring the current density as a function of applied voltage to the thin film electrode (VoltaLab PGZ 100). A platinum wire and an Ag/AgCl electrode were used as the counter and reference electrodes, respectively. Copper strips were used as connectors between the working electrode and source; these were attached to the working electrode using silver paste and taped to the cell with a working area of 1 $cm^2$. Chrono-amperometry was performed for 30 min at potentials ranging from 0.3 V to −0.9 V, and the values obtained were used for reporting the steady state conversion currents. All electrodes were analyzed in phosphate buffer solutions of pH 1, pH 7, and pH 13.

## ■ RESULTS AND DISCUSSION

VPP was carried out in a vacuum oven under the same conditions as previously reported,[27] using the experimental procedure outlined in Figure 1a and b. The resulting thin films of approximately 150 nm thickness contained both PEDOT−Tos and 2D nanomaterials, with plateau regions within the film observed using both AFM and SEM (Figure 1c,d depicts thin films prepared with 0.00255% w/w graphene in the oxidant solution). The images suggest that the nanomaterial is aligned as sheets running parallel to the substrate; the mechanism by which this occurs is not understood. Quantification of the amount of graphene incorporated into the nanocomposite film is difficult, but it is clear from Figure 1c,d that less than complete coverage is observed. It is expected though that the very low % w/w of 2D nanomaterial in the oxidant solutions should not result in a percolating network in the thin film. Furthermore, while microscopy shows that graphene is incorporated into the film, it is clear that it is not present at the air−thin film interface as the Raman spectra shown in Figure S3 demonstrate that the interfacial layer is dominated by the chemistry associated with PEDOT−Tos.

Further support for the presence of graphene in the graphene−PEDOT−Tos film is presented in Figures S3 and S4. Thermogravimetric analysis experiments (Figure S4) were conducted on the VPP PEDOT−Tos with and without graphene. Both materials lose weight below 350 °C, indicating the presence of PEDOT−Tos. Only the graphene−PEDOT−Tos nanocomposite shows a significant amount of material lost above 350 °C, indicating the presence of graphene. The order of magnitude for the weight loss above 350 °C is comparable to

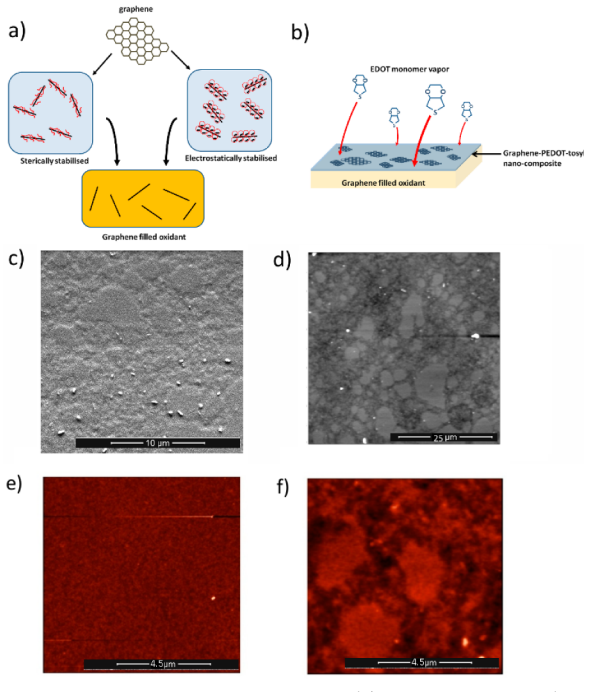


**Figure 1.** Fabrication process of (a) mixing graphene (or other 2D nanomaterial) dispersions with the oxidant solution, which is then (b) coated onto a substrate and exposed to EDOT monomer in the VPP process to create the graphene−PEDOT−Tos nanocomposite thin film. Plateau regions within the resultant nanocomposite film are observed via (c) scanning electron microscopy (25 × 25 $\mu$m area) and (d) atomic force microscopy (50 × 50 $\mu$m area) of graphene−PEDOT−Tos with 0.00255% w/w graphene in the oxidant solution. Comparison of PEDOT−Tos only and graphene−PEDOT−Tos is made by AFM in e and f, respectively, at higher resolution to highlight the plateau structures.

the original weight % dispersed in the oxidant solution. Prior to mixing with the oxidant solution, the graphene dispersion consists as single layers.[44] After dispersing in the oxidant solution and incorporation into PEDOT−Tos, the graphene still remains as single layers, exemplified by a lack of the characteristic peak seen in XRD spectra for multilayer graphene (Figure S3a), combined with the lack of an optical absorbance peak from transmission spectroscopy (Figure S3c). Raman spectroscopy (Figure S3b) yields the same peak structure[50] with and without graphene, and when combined with the AFM observation of comparable nanoscale roughness on and off the plateaus, it indicates that the graphene is effectively buried within the PEDOT−Tos matrix. Given that the graphene is dispersed by the same PEG−PPG−PEG (or similar) copolymers employed to template the growth of the PEDOT−Tos, it is not unreasonable to assume the copolymer also acts in a synergist manner to facilitate the formation of the nanocomposite film.

Electrical analysis of the nanocomposite and the PEDOT−Tos only thin film allows comparison of their conductivity. In the absence of any added water or 2D nanomaterial, the electrical conductivity of the thin film PEDOT−Tos was measured to be ca. 2000 S/cm. The influence of deliberate addition of water to the oxidant solution has previously been reported for the synthesis of VPP PEDOT−Tos thin films.[51] For the study herein, the increasing addition of graphene yields no significant change in electrical properties, with an average electrical conductivity of ca. 2160 S/cm. In contrast, the electrical conductivity linearly decreases to 1000 S/cm for the highest loading of $MoS_2$ studied (0.00111% w/w in the oxidant solution), even though this loading in absolute terms is very low. Ii is important to note here that, irrespective of the trends, these values for the nanocomposite thin films are at least one, if not up to three, orders of magnitude greater than recent attempts to combine graphene and PEDOT.[33,42,43] The conductivity also compares favorably to other recently reported nanocomposite films, including the combination of reduced graphene oxide nanomaterials with silk fibroin as the matrix material.[52] Furthermore, the influence of the added 2D nanomaterials is observed for very low loadings, estimated to be less than that of the parent oxidant solution (<0.00111% w/w). With respect to the nanomaterial−PEDOT−Tos thin film growth, the thickness of the films remains constant irrespective of the loading of $MoS_2$ or graphene.

By comparing the addition of these two different nanomaterials, insight into the influence of 2D nanomaterials can be explored in a manner reported before. It is interesting to note though that there is a measurable difference in the ability of the nanocomposite films to conduct electrical charge depending on the employment of graphene or $MoS_2$. When comparing the 2D nanomaterials, there is an inherent conductivity difference between graphene with ultrahigh conductance and the semiconducting $MoS_2$, suggesting that the presence of the 2D nanomaterial does impart influence on the electrical properties of the nanocomposite. This means that the graphene and $MoS_2$ sheets are not perfectly insulated by the stabilizing copolymer dispersant from the PEDOT−Tos matrix. If correct, this provides a mechanism through which the dispersed 2D nanomaterials can interact with the PEDOT−Tos matrix for enhanced thin film properties.

In parallel with their electrical properties, the mechanical properties of the nanocomposite thin films are of particular interest, including the films' compressive strength and flexural rigidity. From the AFM scan in Figure 2a, the relative compressive strength of the plateau regions where the 2D nanomaterial resides was compared to the surrounding regions (PEDOT−Tos matrix only). The force required to produce an indent or compress the surface (i.e., apparent stiffness) was a factor of 2 greater on the plateaus when compared to the surrounding regions (Figure 2b). Despite the relative nature of this experiment, the results are indicative of a stiffer material such as graphene being present in the plateau region. Based on the Hertz model,[53] a Young's modulus of approximately 8 GPa on the plateau and 4 GPa on the surrounding was calculated. While many instrumental factors contribute to the measured Young's modulus using AFM, these values are on the same order as those reported in the literature for PEDOT films (0.9−2.8 GPa).[54] Importantly, this increase cannot solely be attributed to the VPP PEDOT−Tos, as the thinner film thickness will give rise to a greater contribution from the underlying substrate.[55] Despite this, the measured compressive strength is of the right order of magnitude and clearly indicates a difference in the plateau regions.

In addition to the compressive properties of the nanocomposite film, their flexural properties are of importance, especially when flexible electronic devices are to be considered. Previous studies[56,57] have shown that individual graphene sheets have an exceptionally high in-plane Young's modulus of up to 1 TPa, and their addition to polymers to create nanocomposites has been reported to greatly improve


dx.doi.org/10.1021/cm5014653 | Chem. Mater. 2014, 26, 4207−4213

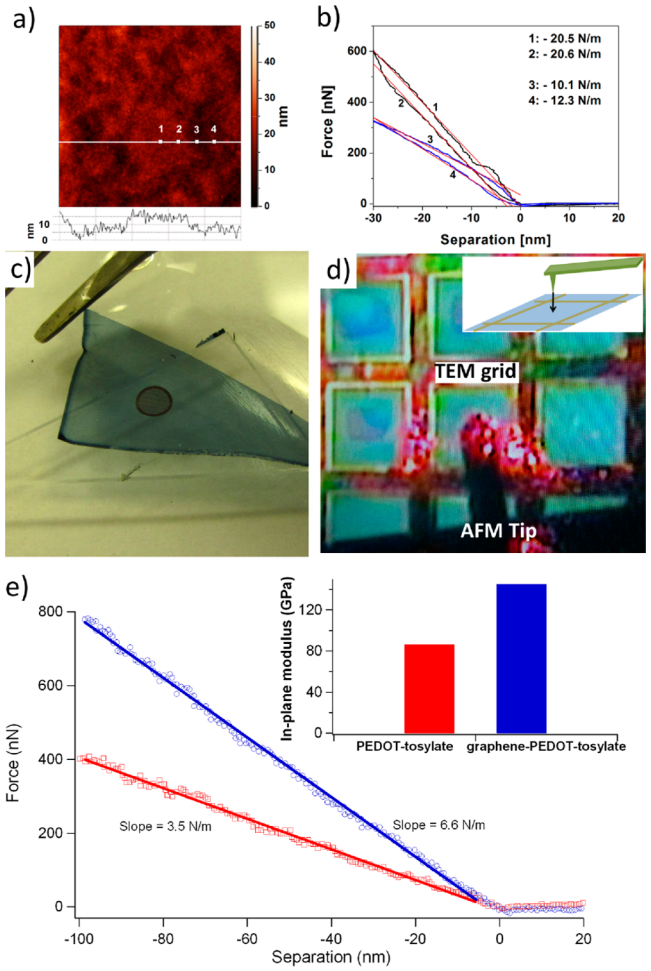


**Figure 2.** Investigation of the mechanical properties of the (0.00255% w/w graphene in the oxidant solution) graphene−PEDOT−Tos nanocomposite film fabricated using VPP. (a) AFM height images (5 × 5 $\mu m^2$ area) show plateau structures of at most 5 nm in height, with lateral dimensions comparable to those of the starting dispersed graphene sheets.[44] The small scale topography is comparable on and off the plateau. (b) Force curves on and off the plateau region show the increase in stiffness on the plateau, owing to the presence of graphene. The force curves in b refer to the points labeled in image a. (c) A TEM grid placed between the free-standing thin film and glass slide substrate during the ethanol rinse of the VPP process. (d) The drum-like structure created by the film over the TEM grid holes in the AFM, with the inset showing a schematic of the AFM experiment. (e) The AFM experiments yield the force vs separation slope, which is required to determine the in-plane modulus of the thin films. The inset in e shows the strengthening of the polymer film by the addition of graphene into the PEDOT−Tos from an in-plane Young's modulus of 86 to 145 GPa.

mechanical properties.[16] Herein, the nanocomposite films were fabricated as free-standing films and interrogated via a nanomechanical technique to determine the in-plane modulus of the films independent of any substrate. The creation of a drum-like structure when the free-standing film is placed over a transmission electron microscope (TEM) Cu 200-mesh grid (Figure 2c) allows the film to be flexed upon application of a force using an AFM tip.[58] By conducting conventional force versus separation experiments at the center of each TEM grid square (Figure 2c,d), the free-standing film's in-plane modulus can be determined from $E_{\text{in-plane}} = D \cdot 12(1 - \upsilon^2)/t^3$, where $D$ is the flexural rigidity (N·m), $\upsilon$ is the Poisson's ratio, and $t$ is the film thickness (m). The flexural rigidity is calculated from the force versus separation experiment as $D = 0.0056 \cdot A^2 \cdot F/S$, where $A$ is the length of the TEM grid edge (m) and $F/S$ (N/m) is the slope of the force versus separation curve (Figure 2e) when the free-standing film is deflected by the AFM tip.[59] For films of comparable thickness fabricated in the same VPP experiment, the in-plane modulus increased from 86 GPa for PEDOT−Tos to 145 GPa for graphene−PEDOT−Tos, a 69% increase (Figure 2e inset). The demonstrated robustness of the nanocomposite films, to be self-supporting, highlights the additional benefit obtained by creating a graphene−PEDOT−Tos composite film. A more detailed discussion relating to the mechanical properties of graphene-based nanocomposites can be found elsewhere.[60]

In many practical applications,[28,29] such materials are exposed to a variety of differing environmental conditions, differing pH being one such example. To understand the impact of pH, the composite thin films were treated with KOH (reduction) and $H_2SO_4$ (oxidation), with visual observation of stability conducted. The images in Figure 3 demonstrate the

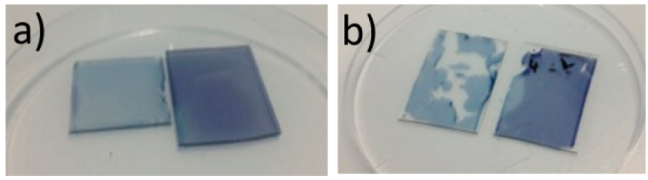


**Figure 3.** Images of oxidation (with $H_2SO_4$) and reduction (with KOH) process. Optical differences are shown for (a) graphene−PEDOT films, which were treated with an acid (transparent to light blue, left) and a base (dark blue, right), and (b) $MoS_2$−PEDOT films treated under the same conditions.

optical differences between acid (left sample in images) and base (right sample in images) treated nanocomposite PEDOT−Tos. It was observed that the acid treatment oxidized the thin films, increasing their transparency, in agreement with typical observations for PEDOT only films.[61] However, after a short time the transparent state decayed back to the ground state, likely due to relaxation of the charge carriers in the polymer back to their equilibrium state. The reduced state is obtained during base treatment, observed as a darkening of the thin films, which does not decay back so readily to the equilibrium state. It is assumed that long exposure to strongly reducing conditions leads to an irreversible reaction, in a similar fashion to that observed for PPy reduced chemically[62] and electrochemically.[63] In agreement with this, in some instances the stability of the nanocomposite PEDOT−Tos thin films was also diminished. Most of the $MoS_2$−PEDOT−Tos acid or base treated films fell apart (Figure 3b); in contrast the graphene−PEDOT−Tos samples showed stability under all conditions (Figure 3a). Thiophene based materials are known to suffer degradation and chain scission from thermal[64] and photochemically[65] induced reactions. At extreme pH, the catalytic property of $MoS_2$ is likely to be enhanced, which may in turn promote redox based degradation of the nanocomposite thin film. A complete understanding of this phenomenon, however, is beyond the scope of the work presented herein and is the subject of further investigation.

Given the relative stability of the graphene−PEDOT−Tos films produced herein, this then warrants further interrogation with respect to their electrical properties upon their chemical


dx.doi.org/10.1021/cm5014653 | Chem. Mater. 2014, 26, 4207−4213

reduction or oxidation. The nanocomposite graphene−PEDOT films started at a conductivity of ca. 2160 S/cm, with chemical reduction leading to a decrease in the electrical conductivity (to 25% of its original value), while chemical oxidation returned no significant change from the as-prepared film. These results indicate that the composite films are close to the fully oxidized state in their "as-deposited" state (i.e., after the VPP process but without pH treatment). To exploit the relatively good (mechanical and electrical) stability of the graphene−PEDOT−Tos films, they were then employed as air electrodes to create and transport energy via an electrocatalytic (oxygen reduction) reaction. In this context, the observation of pH dependence is important as the oxygen reduction reaction consumes protons from within the electrolyte. Variations in the concentration of protons from within the electrolyte thus impact on the efficiency of the reaction by the air-electrode material, and ultimately, the best performing material would be one that showed insensitivity to changing pH. Three different air-electrode performances (graphene−PEDOT−Tos, PEDOT−Tos only, and Pt) were compared in Figure 4 at pH 1, 7, and 13 at an applied voltage of −0.7 V. The full current density versus voltage curves are presented in Figure S5.

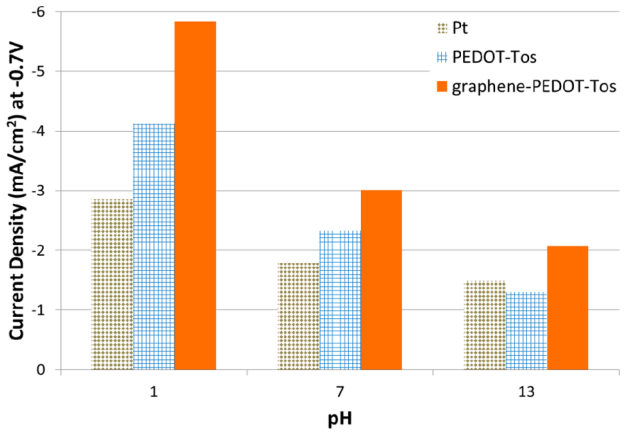


**Figure 4.** Measured steady state conversion current density from the air electrodes at different pH's and −0.7 V. The ORR efficiency is said to increase with increasing current density; in all cases the nanocomposite electrode (solid fill) has the highest ORR efficiency compared to Pt (dot fill) and PEDOT−Tos (line fill).

This comparison shows that the graphene−PEDOT−Tos nanocomposite film studied herein outperforms the Pt air electrode (industry standard material)[66,67] and PEDOT−Tos air electrode (touted replacement for Pt)[28,29,68] for facilitating the oxygen reduction reaction. The increased efficiency with the addition of graphene is hypothesized to be related to the mechanism by which it reduces oxygen being subtly different from the mechanism occurring over Pt.[69] An intermediate metastable state is predicted to occur when using graphene that does not occur for electrocatalytic metals. Boukhvalov and Son show through calculations that as little as 4% atomic defects in the graphene is necessary to reduce the free energy of the ORR process below zero. Coupling this mechanism with the ORR with PEDOT leads to the greater efficiency. The beauty of the graphene−PEDOT−Tos nanocomposite film is the lack of expensive materials, with the electrode consisting of graphene, PEDOT−Tos, and PVDF. Also, the method to fabricate the air electrodes is straightforward (essentially only requiring a vacuum oven); this ease of fabrication complements the benefits of the cheap materials, rather than offsetting the benefits.

## CONCLUSION

There is a strong drive for improving the properties of thin film electrodes employing conducting polymers. In order to produce films with greater mechanical strength without compromising the electrical and electrocatalytic properties, the addition of material to the conducting polymer film to create nanocomposites is gaining increasing attention. Here, nanocomposite films of 2D nanomaterials (graphene and $MoS_2$) in PEDOT−Tos have been prepared using the VPP technique. The VPP technique to incorporate 2D materials into a conducting polymer matrix involves one step; is simple; provides reproducible mechanical, optical, and electrical properties; and has great potential in scaling to large areas. Furthermore, supported films or free-standing films can both be prepared. By dispersing sterically stabilized 2D nanomaterials throughout an oxidant solution containing the same triblock copolymer, the liquid-like properties of the oxidant film, under typical VPP conditions, allowed for the transport of 2D sheets into the forming PEDOT−Tos film. Comparison of the electrical properties for increasing loadings of graphene and $MoS_2$ showed that the resultant conductivity is sensitive to the type of 2D nanomaterial employed, at loadings much less than 0.01% w/w. With respect to the graphene−PEDOT−Tos thin films, they were shown to have a 65% larger in-plane modulus when compared to the polymer only film (at loadings on the order of 0.003% w/w) thereby demonstrating the ability for pristine graphene nanosheets to act as the load distributing component of the composite. The stability of the graphene−PEDOT−Tos transparent conducting films in a variety of pH conditions and higher oxygen reduction efficiency in comparison to Pt and PEDOT−Tos only further confirm the increased performance of these composites prepared using the simple VPP technique.

## ASSOCIATED CONTENT

### Supporting Information

Figures S1−S6. This material is available free of charge via the Internet at http://pubs.acs.org

## AUTHOR INFORMATION

### Corresponding Author

*Phone: +61 8 83025719. Fax: +61 8 8302 3683. E-mail: drew.evans@unisa.edu.au.

### Author Contributions

The manuscript was written through contributions of all authors. All authors have given approval to the final version of the manuscript.

### Notes

The authors declare no competing financial interest.

## ACKNOWLEDGMENTS

G.G.W. acknowledges support from the Australian Research Council (FL110100196). Funding for S.M.N. from the Australian Research Council under the Future Fellowship (ARC FT100100177) program is acknowledged.

## REFERENCES

(1) Hussain, F.; Hojjati, M.; Okamoto, M.; Gorga, R. E. *J. Compos. Mater.* **2006**, *40*, 1511−1575.

(2) Cantwell, W. J.; Morton, J. *Composites* **1991**, *22*, 347−362.
(3) Shi, H.; Liu, F.; Yang, L.; Han, E. *Prog. Org. Coat.* **2008**, *62*, 359−368.
(4) Minelli, M.; De Angelis, M. G.; Doghieri, F.; Marini, M.; Toselli, M.; Pilati, F. *Eur. Polym. J.* **2008**, *44*, 2581−2588.
(5) Watcharotone, S.; Dikin, D. A.; Stankovich, S.; Piner, R.; Jung, I.; Dommett, G. H. B.; Evmenenko, G.; Wu, S.-E.; Chen, S.-F.; Liu, C.-P.; Nguyen, S. T.; Ruoff, R. S. *Nano Lett.* **2007**, *7*, 1888−1892.
(6) Bai, Y.; Cheng, Z. Y.; Bharti, V.; Xu, H. S.; Zhang, Q. M. *Appl. Phys. Lett.* **2000**, *76*, 3804−3806.
(7) Wood, V.; Panzer, M. J.; Chen, J.; Bradley, M. S.; Halpert, J. E.; Bawendi, M. G.; Bulović, V. *Adv. Mater.* **2009**, *21*, 2151−2155.
(8) Prabakar, K.; Seo, H.; Son, M.; Kim, H. *Mater. Chem. Phys.* **2009**, *117*, 26−28.
(9) Coleman, J. N.; Lotya, M.; O'Neill, A.; Bergin, S. D.; King, P. J.; Khan, U.; Young, K.; Gaucher, A.; De, S.; Smith, R. J. *Science* **2011**, *331*, 568−571.
(10) Sham, A. Y. W.; Notley, S. M. *Soft Matter* **2013**, *9*, 6645−6653.
(11) Notley, S. M. *J. Colloid Interface Sci.* **2012**, *375*, 35−40.
(12) Sham, A. Y.; Notley, S. M. *Langmuir* **2014**, DOI: 10.1021/la404745b.
(13) Radisavljevic, B.; Radenovic, A.; Brivio, J.; Giacometti, V.; Kis, A. *Nat. Nanotechnol.* **2011**, *6*, 147−150.
(14) Potts, J. R.; Dreyer, D. R.; Bielawski, C. W.; Ruoff, R. S. *Polymer* **2011**, *52*, 5−25.
(15) Stankovich, S.; Dikin, D. A.; Dommett, G. H.; Kohlhaas, K. M.; Zimney, E. J.; Stach, E. A.; Piner, R. D.; Nguyen, S. T.; Ruoff, R. S. *Nature* **2006**, *442*, 282−286.
(16) Zhao, X.; Zhang, Q.; Chen, D.; Lu, P. *Macromolecules* **2010**, *43*, 2357−2363.
(17) Blake, P.; Brimicombe, P. D.; Nair, R. R.; Booth, T. J.; Jiang, D.; Schedin, F.; Ponomarenko, L. A.; Morozov, S. V.; Gleeson, H. F.; Hill, E. W. *Nano Lett.* **2008**, *8*, 1704−1708.
(18) Notley, S. M. *J. Colloid Interface Sci.* **2013**, *396*, 160−164.
(19) Mak, K. F.; Lee, C.; Hone, J.; Shan, J.; Heinz, T. F. *Phys. Rev. Lett.* **2010**, *105*, 136805.
(20) Splendiani, A.; Sun, L.; Zhang, Y.; Li, T.; Kim, J.; Chim, C.-Y.; Galli, G.; Wang, F. *Nano Lett.* **2010**, *10*, 1271−1275.
(21) Dashora, A.; Ahuja, U.; Venugopalan, K. *Comput. Mater. Sci.* **2013**, *69*, 216−221.
(22) Yue, G.; Wu, J.; Xiao, Y.; Huang, M.; Lin, J.; Lin, J.-Y. *J. Mater. Chem. A* **2013**, *1*, 1495−1501.
(23) Murugan, A. V.; Quintin, M.; Delville, M.-H.; Campet, G.; Gopinath, C. S.; Vijayamohanan, K. *J. Power Sources* **2006**, *156*, 615−619.
(24) Kadantsev, E. S.; Hawrylak, P. *Solid State Commun.* **2012**, *152*, 909−913.
(25) Thakurta, S.; Dutta, A. *J. Phys. Chem. Solids* **1983**, *44*, 407−416.
(26) Quinn, M. D.; Ho, N. H.; Notley, S. M. *ACS Appl. Mater. Interfaces* **2013**, *5*, 12751−12756.
(27) Fabretto, M. V.; Evans, D. R.; Mueller, M.; Zuber, K.; Hojati-Talemi, P.; Short, R. D.; Wallace, G. G.; Murphy, P. J. *Chem. Mater.* **2012**, *24*, 3998−4003.
(28) Winther-Jensen, B.; Winther-Jensen, O.; Forsyth, M.; MacFarlane, D. R. *Science* **2008**, *321*, 671.
(29) Cottis, P.; Evans, D.; Fabretto, M.; Pering, S.; Murphy, P. J.; Hojati-Talemi, P. *RSC Adv.* **2014**, *4*, 9819−9824.
(30) Xia, C.; Advincula, R. C.; Baba, A.; Knoll, W. *Langmuir* **2002**, *18*, 3555−3560.
(31) Fabretto, M.; Autere, J.-P.; Hoglinger, D.; Field, S.; Murphy, P. *Thin Solid Films* **2011**, *519*, 2544−2549.
(32) Hong, W.; Xu, Y.; Lu, G.; Li, C.; Shi, G. *Electrochem. Commun.* **2008**, *10*, 1555−1558.
(33) Choi, K. S.; Liu, F.; Choi, J. S.; Seo, T. S. *Langmuir* **2010**, *26*, 12902−12908.
(34) Chang, H.; Wang, G.; Yang, A.; Tao, X.; Liu, X.; Shen, Y.; Zheng, Z. *Adv. Funct. Mater.* **2010**, *20*, 2893−2902.
(35) Konwer, S.; Boruah, R.; Dolui, S. K. *J. Electron. Mater.* **2011**, *40*, 2248−2255.
(36) Zhang, D.; Zhang, X.; Chen, Y.; Yu, P.; Wang, C.; Ma, Y. *J. Power Sources* **2011**, *196*, 5990−5996.
(37) Bose, S.; Kuila, T.; Uddin, M. E.; Kim, N. H.; Lau, A. K.; Lee, J. H. *Polymer* **2010**, *51*, 5921−5928.
(38) Winther-Jensen, B.; West, K. *Macromolecules* **2004**, *37*, 4538−4543.
(39) Evans, D.; Fabretto, M.; Mueller, M.; Zuber, K.; Short, R.; Murphy, P. *J. Mater. Chem.* **2012**, *22*, 14889−14895.
(40) Fabretto, M.; Müller, M.; Zuber, K.; Murphy, P. *Macromol. Rapid Commun.* **2009**, *30*, 1846−1851.
(41) Bubnova, O.; Khan, Z. U.; Wang, H.; Braun, S.; Evans, D.; Fabretto, M.; Hojati-Talemi, P.; Dagnelund, D.; Arlin, J.-B.; Geerts, Y.; Desbief, S.; Breiby, D.; Andreasen, J. W.; Lazzaroni, R.; Chen, W.; Zozoulenko, I.; Fahlman, M.; Murphy, P.; Berggren, M.; Crispin, X. *Nat. Mater.* **2014**, *13*, 190−194.
(42) Yang, Y.; Li, S.; Zhang, L.; Xu, J.; Yang, W.; Jiang, Y. *ACS Appl. Mater. Interfaces* **2013**, *5*, 4350.
(43) Tung, T. T.; Castro, M.; Feller, J.-F.; Kim, T. Y.; Suh, K. S. *Org. Electron* **2013**, *14*, 2789−2794.
(44) Notley, S. M. *Langmuir* **2012**, *28*, 14110−14113.
(45) Chou, S. S.; Kaehr, B.; Kim, J.; Foley, B. M.; De, M.; Hopkins, P. E.; Huang, J.; Brinker, C. J.; Dravid, V. P. *Angew. Chem.* **2013**, *125*, 4254−4258.
(46) Lotya, M.; King, P. J.; Khan, U.; De, S.; Coleman, J. N. *ACS Nano* **2010**, *4*, 3155−3162.
(47) Hernandez, Y.; Nicolosi, V.; Lotya, M.; Blighe, F. M.; Sun, Z.; De, S.; McGovern, I.; Holland, B.; Byrne, M.; Gun'Ko, Y. K. *Nat. Nanotechnol.* **2008**, *3*, 563−568.
(48) Fontana, I.; Lauria, A.; Spinolo, G. *Phys. Status Solidi B* **2007**, *244*, 4669−4677.
(49) Sader, J. E.; Chon, J. W. M.; Mulvaney, P. *Rev. Sci. Instrum.* **1999**, *70*, 3967−3969.
(50) Garreau, S.; Louarn, G.; Buisson, J.; Froyer, G.; Lefrant, S. *Macromolecules* **1999**, *32*, 6807−6812.
(51) Hojati-Talemi, P.; Bächler, C.; Fabretto, M.; Murphy, P.; Evans, D. *ACS Appl. Mater. Interfaces* **2013**, *5*, 11654−11660.
(52) Hu, K.; Tolentino, L. S.; Kulkarni, D. D.; Ye, C.; Kumar, S.; Tsukruk, V. V. *Agnew. Chem.* **2013**, *52*, 13784−13788.
(53) Hertz, H. *J. Reine Angew. Math.* **1882**, *92*, 156−171.
(54) Lang, U.; Naujoks, N.; Dual, J. *Synth. Met.* **2009**, *159*, 473−479.
(55) Domke, J.; Radmacher, M. *Langmuir* **1998**, *14*, 3320−3325.
(56) Lee, C.; Wei, X.; Kysar, J. W.; Hone, J. *Science* **2008**, *321*, 385−388.
(57) Geim, A. K.; Novoselov, K. S. *Nat. Mater.* **2007**, *6*, 183−191.
(58) Jiang, C.; Markutsya, S.; Pikus, Y.; Tsukruk, V. V. *Nat. Mater.* **2004**, *3*, 721−728.
(59) Harik, I. E.; Salamoun, G. L. *J. Eng. Mech.* **1986**, *112*, 105−118.
(60) Hu, K.; Kulkarni, D. D.; Choi, I.; Tsukruk, V. V. *Prog. Polym. Sci.* **2014**, DOI: 10.1016/j.progpolymsci.2014.03.001.
(61) Tehrani, P.; Hennerdal, L.-O.; Dyer, A. L.; Reynolds, J. R.; Berggren, M. *J. Mater. Chem.* **2009**, *19*, 1799−1802.
(62) Zotti, G.; Schiavon, G.; Comisso, N. *Synth. Met.* **1991**, *40*, 309−316.
(63) Brooke, R.; Evans, D.; Hojati-Talemi, P.; Murphy, P.; Fabretto, M. *Eur. Polym. J.* **2014**, *51*, 28−36.
(64) Verge, P.; Vidal, F.; Aubert, P.-H.; Beouch, L.; Tran-Van, F.; Goubard, F.; Teyssié, D.; Chevrot, C. *Eur. Polym. J.* **2008**, *44*, 3864−3870.
(65) Abdou, M. S.; Holdcroft, S. *Macromolecules* **1993**, *26*, 2954−2962.
(66) Gasteiger, H. A.; Kocha, S. S.; Sompalli, B.; Wagner, F. T. *Appl. Catal., B* **2005**, *56*, 9−35.
(67) Zhang, J.; Sasaki, K.; Sutter, E.; Adzic, R. *Science* **2007**, *315*, 220−222.
(68) Kolodziejczyk, B.; Winther-Jensen, O.; MacFarlane, D. R.; Winther-Jensen, B. *J. Mater. Chem.* **2012**, *22*, 10821−10826.
(69) Boukhvalov, D. W.; Son, Y.-W. *Nanoscale* **2012**, *4*, 417−420.